

New measurement of the relative scintillation efficiency of xenon nuclear recoils below 10 keV

E. Aprile,¹ L. Baudis,² B. Choi,¹ K. L. Giboni,¹ K. Lim,¹ A. Manalaysay,^{2,3,*} M. E. Monzani,¹
G. Plante,¹ R. Santorelli,¹ and M. Yamashita¹

¹*Department of Physics, Columbia University, New York, New York 10027, USA*

²*Physik-Institut, Universität Zürich, CH-8057 Zürich, Switzerland*

³*Department of Physics, University of Florida, Gainesville, Florida 32611, USA*

(Received 29 September 2008; published 22 April 2009)

Liquid xenon is an important detection medium in direct dark matter experiments, which search for low-energy nuclear recoils produced by the elastic scattering of WIMPs with quarks. The two existing measurements of the relative scintillation efficiency of nuclear recoils below 20 keV lead to inconsistent extrapolations at lower energies. This results in a different energy scale and thus sensitivity reach of liquid xenon dark matter detectors. We report a new measurement of the relative scintillation efficiency below 10 keV performed with a liquid xenon scintillation detector, optimized for maximum light collection. Greater than 95% of the interior surface of this detector was instrumented with photomultiplier tubes, giving a scintillation yield of 19.6 photoelectrons/keV electron equivalent for 122-keV γ rays. We find that the relative scintillation efficiency for nuclear recoils of 5 keV is 0.14, staying constant around this value up to 10 keV. For higher energy recoils we measure a value of 0.21, consistent with previously reported data. In light of this new measurement, the XENON10 experiment's upper limits on spin-independent WIMP-nucleon cross section, which were calculated assuming a constant 0.19 relative scintillation efficiency, change from $8.8 \times 10^{-44} \text{ cm}^2$ to $9.9 \times 10^{-44} \text{ cm}^2$ for WIMPs of mass 100 GeV/ c^2 , and from $4.5 \times 10^{-44} \text{ cm}^2$ to $5.6 \times 10^{-44} \text{ cm}^2$ for WIMPs of mass 30 GeV/ c^2 .

DOI: [10.1103/PhysRevC.79.045807](https://doi.org/10.1103/PhysRevC.79.045807)

PACS number(s): 29.40.Mc, 78.70.-g, 95.35.+d, 61.25.Bi

I. INTRODUCTION

Numerous observations point to the existence of a nonluminous, nonbaryonic component of our universe known as dark matter [1–3]. This matter could be in the form of a new type of particle [4,5] whose existence can be naturally explained as a thermal relic of the Big Bang. Such a particle, which would likely be massive and electrically neutral, is commonly referred to as a weakly interacting massive particle (WIMP). There are currently a number of efforts, worldwide, to directly detect WIMPs in terrestrial particle detectors [6–10]. These are sensitive to nuclear recoils below 100 keV [11,12] and take advantage of the fact that WIMPs, interacting primarily with atomic nuclei, would be distinguishable from the predominantly electromagnetic backgrounds present in such experiments.

Although there are varying strategies in this direct detection search, liquid xenon (LXe) has recently come to the forefront of the field as a powerful detection medium [8–10]. When particles interact in LXe, they produce prompt scintillation photons and ionization [13] that can be measured simultaneously to infer the energy and the type of interaction. The scintillation emission spectrum from LXe is singly peaked at 178 nm with a width of 13 nm [14]. The *scintillation yield*, defined as the number of photons produced per unit energy, depends on the identity of the particle depositing the energy [15,16]. Because WIMPs primarily interact with atomic nuclei, in LXe searches the quantity of interest is the scintillation yield of recoiling xenon nuclei. The recent XENON10 measurement [9,10] has pushed the energy threshold of LXe detectors

down to regions where the nuclear recoil scintillation yield is poorly understood. This lack of knowledge is the source of XENON10's largest systematic uncertainty.

Measurement of the absolute scintillation yield of any particle species is quite difficult, so instead relative yields are often reported. Monoenergetic γ rays of 122 keV from ^{57}Co are commonly used to calibrate the electronic recoil energy scale. The scintillation yield of nuclear recoils *relative* to that of 122-keV γ rays is known as the relative scintillation efficiency, or \mathcal{L}_{eff} , and a new measurement of this energy-dependent value is reported herein. Although the absolute scintillation yield of electronic recoils is not linear in energy [17], the 122-keV γ rays provide an anchor point upon which one can base scintillation yields of all other energies and species.

II. EXPERIMENTAL SETUP

A. Neutron beam

The determination of \mathcal{L}_{eff} requires the production of nuclear recoils whose energies are known independent of their response in the LXe. Nearly monoenergetic neutrons, produced in a $T(p, n)^3\text{He}$ reaction, are incident on a LXe detector. Some of the neutrons that scatter under an angle θ are detected by an EJ301 organic liquid scintillator detector [18] (see Fig. 1), capable of distinguishing electronic (γ rays) from nuclear (neutron) recoils via pulse shape discrimination (PSD) [19,20]. In this way, the energy of the recoiling Xe nucleus is known kinematically and is given by the relation

$$E_r \approx 2E_n \frac{m_n M_N}{(m_n + M_N)^2} (1 - \cos \theta), \quad (1)$$

* Corresponding author: aaronm@physik.uzh.ch

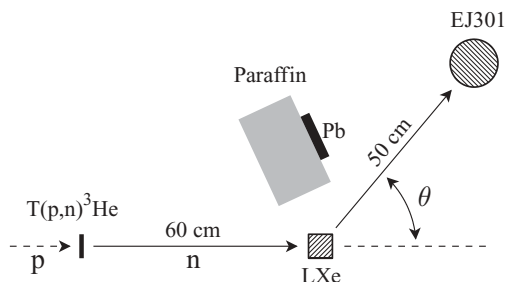


FIG. 1. Schematic diagram of the experimental setup. Incoming 1-MeV neutrons scatter in the LXe detector and are tagged by the EJ301 neutron scintillator for different scattering angles of 48° , 62° , 70.5° , and 109.5° . The paraffin and lead are used to shield the EJ301 neutron scintillator from direct neutrons and γ rays.

where E_r is the recoil energy, E_n is the energy of the incoming neutron, m_n and M_N are the masses of the neutron and nucleus, respectively, and θ is the scattering angle (the approximation is valid when $M_N \gg m_n$ and $E_n \ll m_n c^2$).

The measurements were conducted in the neutron beam of the Radiological Research Accelerator Facility at the Columbia Nevis Laboratory, also described in a previous study of \mathcal{L}_{eff} [21]. In the present work, 1.9-MeV protons were incident on a tritium target, yielding 1-MeV neutrons. The $T(p, n)^3\text{He}$ reaction produces neutrons over 4π sr; however, the luminosity is peaked in the forward direction and the energy variation due to the angular spread of the 1-in. LXe detector cell, 60 cm distant from the tritium target, was less than 0.09% [22]. The incident proton energy, E_p , was known to within 0.1%. These two systematic uncertainties, coming from the angular dependence of E_n and the uncertainty in E_p , are considered negligible and are not included in the calculations of subsection III B. The dominant spread in the incident neutron energy comes from the thickness of the tritium target and was estimated to give a $1\text{-}\sigma$ spread of $\pm 7.8\%$ [23]. An additional component to the spread in E_r comes from the finite size of both detectors, which leads to an uncertainty in the true scattering angle, θ . These uncertainties were determined by Monte Carlo (MC) simulations and are included in the uncertainties in Table I.

Also seen in Fig. 1, a 30-cm-thick paraffin block was placed along the line of sight between the tritium target and the EJ301 scintillator to block neutrons from directly interacting in the EJ301. In addition to the paraffin block, 5 cm of Pb shielded the EJ301 from γ s produced in the target. The data presented here were accumulated in several data sets with the following neutron-scattering angles: 48° , 62° , 70.5° , and 109.5° .

B. Detector design

The LXe detector was designed to allow a zero-field measurement of the scintillation light with very high efficiency, covering $>95\%$ of the interior surface with photon detectors. The design also minimizes the amount of LXe outside the active volume to reduce the background from interactions in this passive scintillation layer. A schematic of the detector design is seen in Fig. 2. The LXe volume is viewed by six 1-in.-square

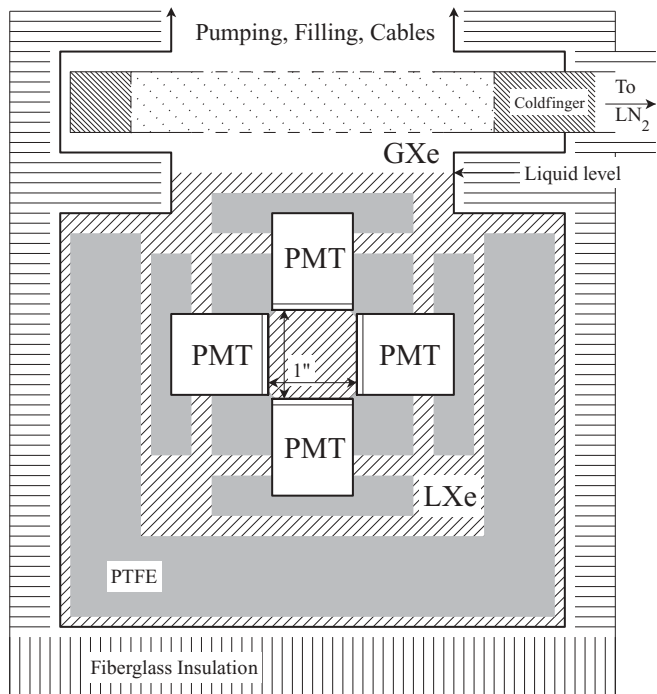


FIG. 2. Schematic diagram of the LXe detector used for the \mathcal{L}_{eff} measurement. Visible are four of the six PMTs used to view the 1-in.³ active LXe volume.

Hamamatsu metal channel R8520-06-Al photomultiplier tubes (PMTs), sensitive to the 178-nm Xe scintillation. Four of these PMTs use a new bialkali photocathode, with a quantum efficiency around 40% at room temperature [24]. The PMTs, held together with a polytetrafluoroethylene (PTFE) frame, form a cube such that each PMT window covers a face of the cube. Both the photocathode and metal body of the PMTs are held at ground potential, with positive high voltage applied to the anodes. This configuration guarantees that no residual electric fields exist in the LXe, whose scintillation yield strongly depends on the applied field [25] (by definition, \mathcal{L}_{eff} is the relative light yield at zero field). The PMT assembly is mounted in a stainless steel vessel, surrounded by fiberglass for thermal insulation.

Xe gas, purified by the same system used in Ref. [21], is liquefied in the vessel, cooled by a copper ring cold finger thermally coupled to a liquid nitrogen bath. The LXe level is kept above the top PMT and the temperature was held constant at 180K (the same T and P as in XENON10 [9,10]), with fluctuations less than 0.03%. A total of 2.5 kg of Xe was used.

The EJ301 scintillator is contained in an aluminum cylinder 3 in. in diameter and 3 in. tall, viewed by a single Photonic XP4312B PMT and read out with the same electronics as the PMTs in the LXe detector.

C. Data acquisition and processing

The PMT signals are fed into an amplifier, with two identical outputs per input channel. One output is digitized by a 100 MHz flash ADC, while the other output is fed to the triggering system.

For the trigger, the six LXe PMT channels are combined in pairs to form three trigger channels, each discriminated at a level of 0.3 photoelectrons (p.e.). The logical outputs of the three discriminator channels are passed to an $N = 3$ coincidence unit. The efficiency of this trigger condition, determined by the Monte Carlo method, is $\sim 100\%$ at 20 p.e., slowly rolling off to $\sim 90\%$ at 10 p.e.. The EJ301 trigger is taken simply as the output of the discriminated signal.

For the measurement of the neutrons' time-of-flight (TOF) the LXe trigger is fed directly to the "start" input of a time-to-amplitude converter (TAC), whereas the EJ301 trigger provides the "stop" after appropriate delay. The output of the TAC is digitized by the same flash ADC unit. Calibration of the TOF signal is discussed in subsection III A.

The shape of the signal in the EJ301 depends on the incoming particle species and can be used to distinguish neutrons from γ rays because the characteristic scintillation decay time is different for these particles. As a result, the tails of pulses resulting from nuclear recoils will be characteristically longer than those from electronic recoils. A description of the mechanisms involved in this process can be found in Ref. [19]. In EJ301, the "slow" component is two orders of magnitude longer than the "fast" component, reported to be 3.2 ns [18]. A PSD parameter is constructed by dividing the area under the pulse's tail by the total area of the pulse, with the tail defined as the part of the trace starting 30 ns after the peak until the trace reaches 5% of the peak value.

III. DATA ANALYSIS AND RESULTS

A. Calibrations

The PMTs were calibrated *in situ* with a pulsed blue LED to measure and monitor the gain. The light from the LED produces a single p.e. spectrum, whose mean determines the gain of the multiplier chain. With a complete set of such LED calibration measurements, the signals obtained for all acquisitions can be converted to a value in number of p.e.. The relationship between the number of collected p.e. and the total number of emitted photons depends on the geometrical light collection efficiency, the quantum efficiency of the photocathodes, and the collection efficiency between the photocathode and the first dynode. Although these values are not known to very high precision, they represent completely linear processes and hence lead to a linear relationship between the total number of scintillation photons and the measured number of p.e.. Comparing the p.e. yields of various sources thus gives a measure of their relative scintillation yields.

As \mathcal{L}_{eff} is defined relative to the scintillation yield of 122-keV γ rays, data from a 100 μCi ^{57}Co source were taken periodically during the experiment. Figure 3 shows the spectrum from one such calibration. The ^{57}Co yield was measured to be 19.64 ± 0.07 (stat) ± 0.11 (sys) p.e./keV, where the statistical uncertainty is the combination of the parameter uncertainties of the fits from the various calibration data, and the systematic uncertainty is taken from the variation in this yield over the two-day duration of the experiment. One set of PMT gain values was applied to all data, and thus the

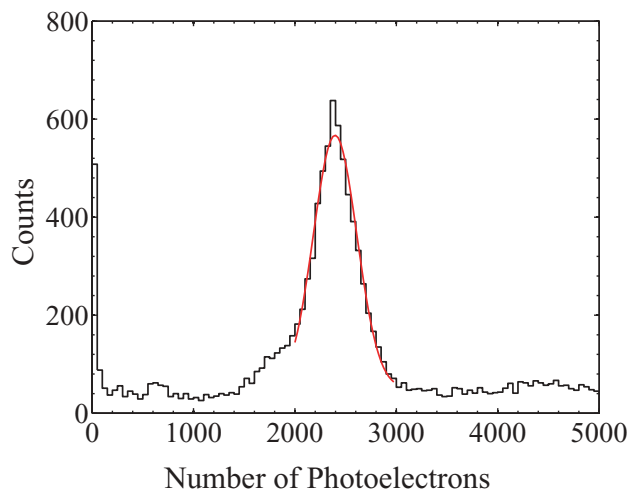


FIG. 3. (Color online) The scintillation light spectrum of 122-keV γ rays from ^{57}Co , used to calibrate the electronic recoil energy scale. This calibration gives a scintillation yield of 19.64 p.e./keV.

systematic uncertainty in the ^{57}Co yield quoted above accounts for both variations in yield and PMT gain.

In addition to ^{57}Co , data were also collected from a ^{22}Na source. This source emits a β^+ that promptly loses energy in the Na and annihilates, producing two 511-keV γ rays emitted simultaneously in opposite directions. With the source placed between the LXe detector and the EJ301 detector, the two γ rays will interact at essentially the same time in the two detectors. In this way, ^{22}Na provides a baseline TOF = 0 that, when used in conjunction with a variable delay generator, is used to calibrate the TOF measurement system.

B. Event selection, backgrounds, and results

The processing of the data acquired at each angle yields two parameters that can be used to select events of interest: the event TOF and the PSD parameter from the EJ301 neutron detector. Figure 4 shows the distribution of events in PSD parameter and TOF. Clearly visible are the nuclear recoil and electronic recoil bands, in addition to the peaks from both γ and neutron scatters. The PSD cut is chosen to accept a majority of the nuclear recoil band while rejecting electronic recoils. The width of the TOF cut is 10 ns, which is the expectation based on the spread in E_n and the finite size of the detectors. The tail of the TOF peak is due mainly to events where the neutron scattered in one of the detector materials in addition to the LXe, before interacting in the EJ301 scintillator. Multiple scatters in the LXe also add to the tail, although MC simulations indicate that their overall contribution is less than 2%.

Two backgrounds contribute to the LXe spectrum that cannot be vetoed with the cuts described above and must instead be subtracted. It is clear from Fig. 4 that beneath the neutron peak lies a population of events that have a flat TOF spectrum. These are identified as neutrons that accidentally interacted in the EJ301 in coincidence with an unrelated event

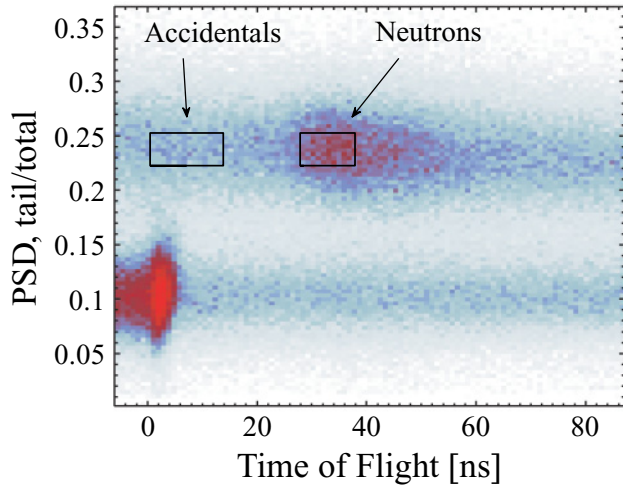


FIG. 4. (Color online) The distribution of triggered events in PSD vs. TOF space from the data set at 70.5° . An “upper” band and “lower” band are readily identifiable in the data and correspond to nuclear recoils and electronic recoils, respectively. The peak at the lower left near $\text{TOF} = 0$, due to γ rays that Compton scatter in the LXe before striking the EJ301, is easily vetoed by the PSD cut. A population of accidental triggers (see text) having a flat TOF spectrum is visible in both bands and contributes background events within the neutron peak. The LXe spectra of events within the left box are used as the expectations of this background. The width of the right box (10 ns) is chosen to accept neutrons that interact in any region of the finitely sized detectors.

in the LXe and are referred to as accidentals. As these events are uniform in TOF space, accidentals outside of the TOF peak should have the same energy spectrum as those within the peak. The LXe spectrum of the events inside the box of Fig. 4 labeled “accidentals” was used as the expectation of the accidentals background. The region to the left of the peak was chosen because the peak’s extended tail contaminates the accidentals spectrum to the right of the “neutron” peak.

The second background that cannot be vetoed comes from neutrons that scattered in various detector materials in addition to the LXe, before interacting in the EJ301. Here referred to as materials background, MC simulations show that the spectrum of these events in the LXe follows an approximately exponential distribution in the region of the peak. Figure 5(a) displays the results of the MC simulation of the data set at 70.5° , indicating the contribution from the materials background. To estimate the spectrum of these events in the real data, a decaying exponential was fit to the high-energy portion of the distributions after subtracting the accidentals background.

After applying cuts (PSD and TOF) and subtracting backgrounds (accidentals and materials), a spectrum results in which the peak from single-scatter neutrons can be readily identified, seen as the solid circles in Fig. 6. The horizontal scale of these spectra is given as “keVee” meaning “keV electron-equivalent,” indicating it is the energy scale derived from the ^{57}Co calibration. \mathcal{L}_{eff} is found from the following

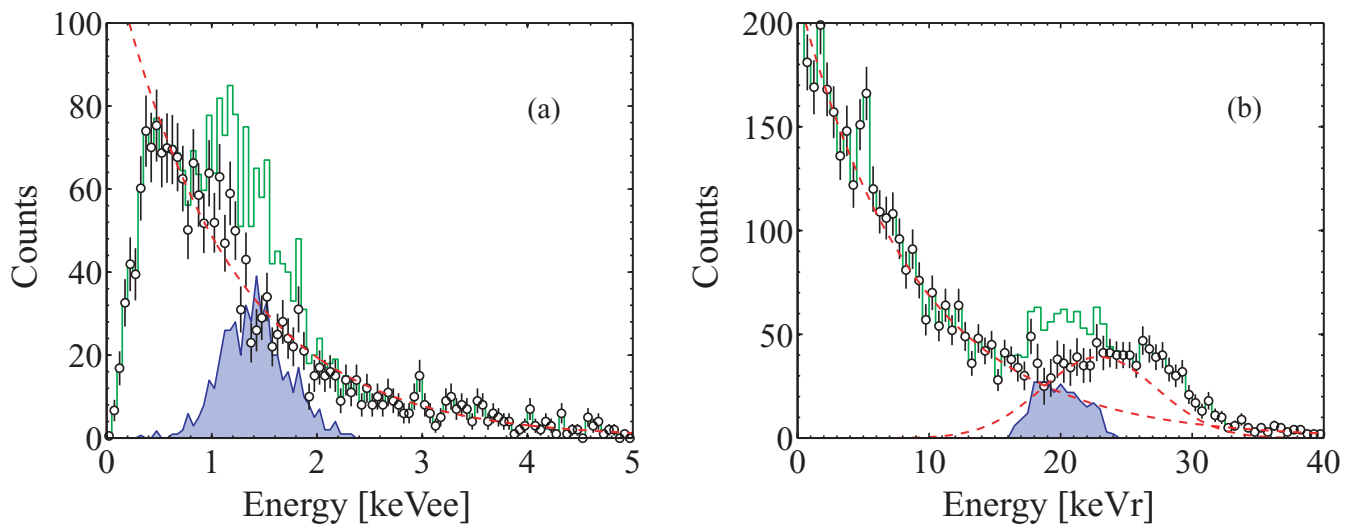


FIG. 5. (Color online) Selected results of the Monte Carlo simulations, which do not include the accidentals background. (a) The spectrum of events tagged at 70.5° , scaled with the measured value of \mathcal{L}_{eff} giving the electron-equivalent energy (keVee), convoluted assuming Poisson statistics for the number of p.e. and multiplied by the simulated trigger efficiency curve. The green histogram is the total spectrum, and the black circles indicate the true materials background. The red dashed line is an exponential fit to the high-energy region of the green histogram; its agreement with the true materials background confirms the validity of this technique’s use in the real data. The shaded blue area shows the spectrum of true elastic single scattered neutrons. (b) The spectrum of events tagged at 109.5° . The data are shown in the original, recoil equivalent energy scale (keVr) without Poisson convolution. The materials background in this region departs from the exponential behavior seen at lower energies and distorts the position of the peak from true single scatters, at 20 keV. The red dashed lines are the result of an exponential+Gaussian fit. The Gaussian component, centered at 22.94 ± 4.34 keV, is used as the “true” energy of the Gaussian component in the real spectrum.

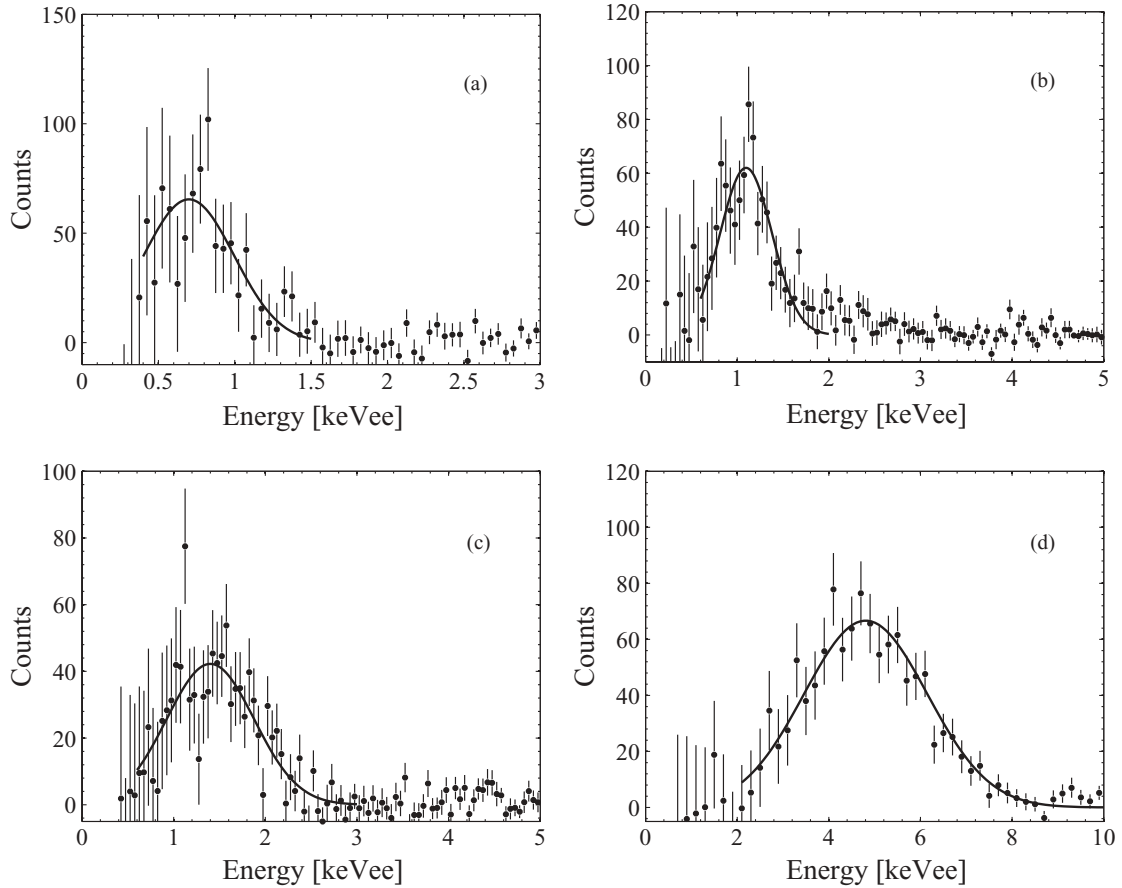


FIG. 6. Energy spectrum measured at the four angles used in this study: (a) -48° , (b) -62° , (c) -70.5° , and (d) -109.5° . The data are shown after subtracting both accidentals and materials backgrounds. Error bars are the combined errors of the original spectra, accidentals, and materials background, included in the Gaussian fits indicated by the solid curves.

relation:

$$\mathcal{L}_{\text{eff}} = \frac{E_{\text{ec}}}{E_{\text{nr}}}, \quad (2)$$

where E_{ec} is the electron-equivalent energy (based on the 122 keV scintillation yield) and E_{nr} is the true recoil energy. Thus, when these spectra are fit with Gaussian functions, the estimators of the mean, divided by the true recoil energy, give the \mathcal{L}_{eff} values at these energies.

The uncertainties in the recoil energies are taken directly from the spread in the incident neutron energy combined with the geometrical uncertainty due to the finite size of the detectors. These values were obtained from the MC simulations and are listed in the second column of Table I. The uncertainties in \mathcal{L}_{eff} were calculated by considering the spread in E_r mentioned above, statistical errors in the Gaussian fits, the variation in ^{57}Co light yield, the uncertainty in the background estimations, and the effect of the trigger threshold roll-off. This last uncertainty was calculated by finding the peak positions before and after dividing the spectra by the trigger efficiency discussed in subsection II C. However, only the lowest angle (48°) was affected by this trigger roll-off. The asymmetric error bars of the 5-keV data point is due to both the trigger roll off and the actual parameter

uncertainty in the Gaussian fit. For all angles, the dominant contribution to the uncertainty in \mathcal{L}_{eff} is from the spread in E_r .

Though the purpose of this study was to investigate the behavior of \mathcal{L}_{eff} below 10 keV, it was necessary to collect data from higher-energy recoils to establish a connection with previous studies. For this, the EJ301 was placed at a scattering angle of 109.5° , corresponding to 20.0 keV recoils. However, this angle is close to the minimum in the differential scattering cross section of 1 MeV neutrons in Xe [26], and so the signal from “true” single scatters is well below the background. Additionally, the materials background in this energy range departs from a decaying exponential. As can be seen in the MC data of Fig. 5(b), the actual “bump” in the spectrum, coming primarily from neutrons that have also scattered in the PTFE, is actually slightly higher than 20 keV. To find the true energy of the peak position, the same procedure used in examining the real data was applied here to the MC data, giving a recoil energy of 22.94 ± 4.34 keV. The spread in E_r was taken as the width of the Gaussian component in the MC spectrum.

The values obtained for \mathcal{L}_{eff} are listed in Table I and additionally shown in Fig. 7 along with the results of previous studies [21,27–30].

TABLE I. The values of \mathcal{L}_{eff} obtained at the four angles used in this study. Error bars on the recoil energies are the spread of E_n as mentioned in subsection II A combined with the geometrical uncertainties. The uncertainties in \mathcal{L}_{eff} are the combination of all statistical and systematic errors mentioned in the text.

θ	E_r (keV)	\mathcal{L}_{eff}
48°	5 ± 0.68	$0.141^{+0.025}_{-0.037}$
62°	8 ± 0.91	0.137 ± 0.016
70.5°	10 ± 1.06	0.140 ± 0.016
109.5°	22.94 ± 4.34	0.205 ± 0.039

IV. DISCUSSION OF RESULTS

The data point from the measurement at 109.5° shows agreement with other measurements whose high-energy behavior averages out to $\mathcal{L}_{\text{eff}} \approx 0.19$. Below 10 keV, our values are substantially lower than the central values of Chepel *et al.* [27], with a considerable improvement in precision. The central value at 10 keV is consistent with the lowest-energy data point of Aprile *et al.* [21], enforcing the accuracy of this measurement. Unfortunately, the theoretical models of neither Lindhard [15] nor Hitachi [16] can shed any light on the behavior of \mathcal{L}_{eff} in this energy range. Hitachi's model, which attempts to take into account incomplete charge recombination and additional electronic quenching, is based on Lindhard quenching as well as the Thomas-Fermi approximation; for Xe nuclear recoils, both break down below 10 keV [32,33].

As mentioned in the Introduction, the uncertainty in \mathcal{L}_{eff} at low recoil energies presents the largest systematic uncertainty in the results of the XENON10 dark matter experiment, where

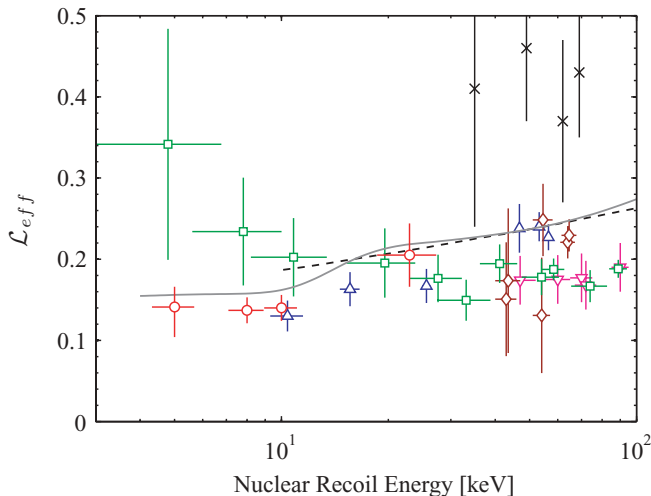


FIG. 7. (Color online) Measured \mathcal{L}_{eff} values as a function of Xe nuclear recoil energy. Symbols correspond to (○) this work; (□) Chepel *et al.* [27]; (△) Aprile *et al.* [21]; (◇) Akimov *et al.* [28]; (×) Bernabei *et al.* [29]; (▽) Arneodo *et al.* [30]. The solid gray curve is the result from a recent best-fit analysis of XENON10 AmBe source data and MC [31]. Also shown is the theoretical prediction of Hitachi (dashed line) [16].

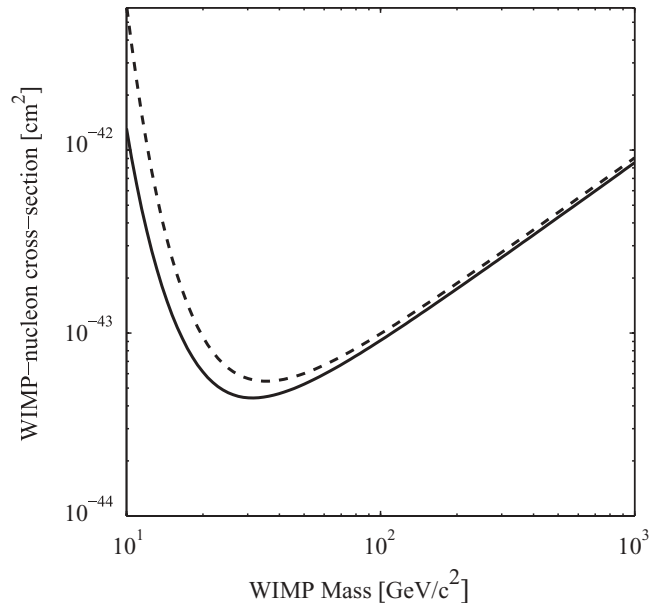


FIG. 8. The upper limit on the WIMP-nucleon spin-independent cross section based on the 58.6 live days of XENON10's WIMP search, shown with a flat $\mathcal{L}_{\text{eff}} = 0.19$ (solid). An \mathcal{L}_{eff} function consistent with the results of this study, applied to the same XENON10 data is shown as well (dashed).

it was chosen to use a flat $\mathcal{L}_{\text{eff}} = 0.19$ as a compromise between the seemingly opposing trends observed by Chepel and Aprile. Under this assumption, the WIMP-nucleon spin-independent cross section for WIMPs of mass 100 GeV/c^2 was constrained to be less than $8.8 \times 10^{-44} \text{ cm}^2$ and $4.5 \times 10^{-44} \text{ cm}^2$ at 30 GeV/c^2 , indicated by the solid curve in Fig. 8. Allowing for \mathcal{L}_{eff} scenarios below 20 keV that cover the values allowed by both Chepel and Aprile gives upper limits that vary by $\sim 40\%$ at 30 GeV/c^2 and $\sim 18\%$ at 100 GeV/c^2 , with variations becoming less severe with increasing WIMP mass. With an \mathcal{L}_{eff} model that follows the new data points of this study, the resulting upper limit is shown in Fig. 8 as the dashed curve. The limit is shifted up to $9.9 \times 10^{-44} \text{ cm}^2$ and $5.6 \times 10^{-44} \text{ cm}^2$ for WIMPs of mass 100 GeV/c^2 and 30 GeV/c^2 , respectively.

It has become clear from XENON10 that future dark matter searches using LXe must have sensitivity to nuclear recoils below 10 keV to be competitive. The improved understanding of \mathcal{L}_{eff} 's behavior presented in this study not only permits a more precise interpretation of XENON10's results but also benefits future dark matter searches also using LXe. Several next-generation LXe dark matter searches are currently in operation or under construction, such as XENON100 [34], LUX [35], and XMASS [36]. These experiments will begin to probe for the first time those regions of parameter space most favored by many theoretical models and will consequently rely quite heavily on a precise understanding of LXe's scintillation efficiency for low-energy nuclear recoils when interpreting their results. This is true in the case of a null result and especially in the case of a positive signal. If and when such a signal is detected, a measurement of the WIMP mass, for

example, which relies on analyzing the energy spectrum of recoils, will be affected by the precision to which \mathcal{L}_{eff} is known.

V. SUMMARY

The work presented here represents a new measurement of \mathcal{L}_{eff} in an energy range where it is poorly understood but highly important to the field of dark matter direct detection with liquid xenon detectors. We show that at 10 keV and below, this efficiency is lower than the average value of $\mathcal{L}_{\text{eff}} = 0.19$ while the measurement in the literature [27] suggests a *rise* in \mathcal{L}_{eff} at these energies, albeit with large errors. In light of the results of our measurement, the XENON10 spin-independent limit is shifted up for WIMPs of mass 100 GeV/ c^2 by 12.5%, while the high-mass regime is relatively unchanged.

ACKNOWLEDGMENTS

We acknowledge the University of Florida High-Performance Computing Center for providing computational resources that have contributed to the simulations reported within this article. This work was funded by National Science Foundation Grants Nos. PHY-03-02646 and PHY-04-00596 and by the Swiss National Foundation Grant No. 20-118119. Additional support was provided by Grant No. P41 EB002033-13, Radiological Research Accelerator Facility (RARAF), from the National Institutes of Health/National Institute of Biomedical Imaging and Bioengineering (NIBIB). We express our gratitude to Dr. Steve Marino of RARAF for the beam time and his support throughout the measurements.

-
- [1] K. G. Begeman, A. Broeils, and R. H. Sanders, *Mon. Not. R. Astron. Soc.* **249**, 523 (1991).
- [2] D. N. Spergel *et al.* (WMAP Collaboration), *Astrophys. J. Suppl. Ser.* **170**, 377 (2007).
- [3] D. Clowe *et al.*, *Astrophys. J. Lett.* **648**, L109 (2006).
- [4] G. Jungman, M. Kamionkowski, and K. Griest, *Phys. Rep.* **267**, 195 (1996).
- [5] G. Bertone, D. Hooper, and J. Silk, *Phys. Rep.* **405**, 279 (2005).
- [6] R. J. Gaitskell, *Annu. Rev. Nucl. Part. Sci.* **54**, 315 (2004).
- [7] L. Baudis, *Int. J. Mod. Phys. A* **21**, 1925 (2006).
- [8] G. J. Alner *et al.* (ZEPLIN II Collaboration), *Astropart. Phys.* **28**, 287 (2007).
- [9] J. Angle *et al.* (XENON Collaboration), *Phys. Rev. Lett.* **100**, 021303 (2008).
- [10] J. Angle *et al.* (XENON Collaboration), *Phys. Rev. Lett.* **101**, 091301 (2008).
- [11] J. R. Primack, D. Seckel, and B. Sadoulet, *Annu. Rev. Nucl. Part. Sci.* **38**, 751 (1988).
- [12] J. D. Lewin and P. F. Smith, *Astropart. Phys.* **6**, 87 (1996).
- [13] T. Doke, K. Masuda, and E. Shibamura, *Nucl. Instrum. Methods A* **291**, 617 (1990).
- [14] J. Jortner *et al.*, *J. Chem. Phys.* **42**, 4250 (1965).
- [15] J. Lindhard *et al.*, *Mat. Fys. Medd. Dan. Vid. Selsk.* **33**, 10 (1963).
- [16] A. Hitachi, *Astropart. Phys.* **24**, 247 (2005).
- [17] M. Yamashita *et al.*, *Nucl. Instrum. Methods A* **535**, 692 (2004).
- [18] <http://www.eljentechnology.com>; EJ301 is a proprietary name for C₆H₄(CH₃)₂, which is also known by the proprietary names BC501A and NE213.
- [19] G. F. Knoll, *Radiation Detection and Measurement*, 3rd ed. (Wiley & Sons, Inc., New York, 2000).
- [20] S. Marrone *et al.* (n-TOF Collaboration), *Nucl. Instrum. Methods A* **490**, 299 (2002).
- [21] E. Aprile *et al.*, *Phys. Rev. D* **72**, 072006 (2005).
- [22] H. Liskien and A. Paulsen, *Nucl. Data Tables* **11**, 569 (1973).
- [23] Steve Marino (personal communication, 2007).
- [24] http://jp.hamamatsu.com/resources/products/etd/eng/html/pmt_003.html. The photocathodes used in this study were specially designed to have their peak sensitivity near 178 nm, the wavelength of Xe scintillation light.
- [25] E. Aprile *et al.*, *Phys. Rev. Lett.* **97**, 081302 (2006).
- [26] M. B. Chadwick *et al.*, *Nucl. Data Sheets* **107**, 2931 (2006), <http://www.nndc.bnl.gov/exfor/endlf00.htm>.
- [27] V. Chepel *et al.*, *Astropart. Phys.* **26**, 58 (2006).
- [28] D. Akimov *et al.*, *Phys. Lett.* **B524**, 245 (2002).
- [29] R. Bernabei *et al.*, *EPJdirect C* **11**, 1 (2001).
- [30] F. Arneodo *et al.*, *Nucl. Instrum. Methods A* **449**, 147 (2000).
- [31] P. Sorensen *et al.*, *Nucl. Instrum. Methods A* **601**, 339 (2009).
- [32] A. Hitachi, *J. Phys.: Conf. Ser.* **65**, 012013 (2007).
- [33] A. Mangiarotti *et al.*, *Nucl. Instrum. Methods A* **580**, 114 (2007).
- [34] E. Aprile, in the proceedings of Identification of Dark Matter 2008, PoS(idm2008) 018; <http://pos.sissa.it/POSreaders.html>.
- [35] R. Gaitskell, in the proceedings of Identification of Dark Matter 2008, PoS(idm2008) 015; <http://pos.sissa.it/POSreaders.html>.
- [36] Y. Suzuki, in the proceedings of Identification of Dark Matter 2008, PoS(idm2008) 001; <http://pos.sissa.it/POSreaders.html>.